Thermal Conductance of Interleaving Fins

Michiel A. J. van Limbeek[1,2,*] and S. Vanapalli[1]

[1] *Energy Materials and Systems Group, Department of Science and Technology, University of Twente, 7500 AE Enschede, Netherlands*

[2] *Max Planck Institute for Dynamics and Self-Organization, 37077 Göttingen, Germany*

(Received 16 August 2019; revised manuscript received 15 October 2019; published 20 December 2019)

Interleaving fins can significantly increase heat transfer by increasing the effective area per unit base area. The fins are separated uniformly by a gap, which is filled with a flow medium to control the heat flux. The heat flux between the plates depends strongly on the thermal conductivity of the fin material and the medium between them, as well as the dimensions. In earlier studies, an empirical fitting method has been used to determine the total effectiveness of the fins. However, it required complete characterization of the fins for each new set of operating conditions. In this paper, a simplified analytical model is developed, which still preserves the main physical traits of the problem. This model reveals the dimensionless parameter group containing both the material properties and the fin geometry that govern the heat transfer. Rigorous testing of the model using a numerical finite-element model shows an accuracy within 2% over a large parameter space, varying both dimensions and material properties. Lastly, this model is put to the test with previously measured experimental data and good agreement is obtained.

DOI: 10.1103/PhysRevApplied.12.064048

I. INTRODUCTION

Temperature control is essential in many situations: from regulating the body temperature of biological species to keeping your drinks cold in your fridge and preventing your computer from overheating. Whereas rapid heating can be easily achieved by resistive electrical heating, rapid cooling is more complicated, as heat needs to be transported toward a heat sink. Many cases use conduction for transport, for which the thermal conductance is constant. For some cases, however, this is not desirable and one wants to regulate the conductance, that is, change the conductance over time.

As an example, in hyperpolarized molecular magnetic-resonance-imaging (MRI) systems, the sample sleeves that accommodate variable-temperature inserts are integrated into the cryostat structure. This requires the entire system to be warmed up for servicing. A heat switch has been used in a recent development to thermally disconnect the sample sleeve from the cold plate for quick servicing [1]. Another common example is a thermal battery, where some (phase-change) material [2–5] is used to maintain a desired operating-temperature window for the instrument. The battery should be thermally coupled to a cold sink to charge the system [6]. *In situ* cryofixation of cells is of growing interest in phase-contrast microscopy for studying dynamic cellular processes associated with physiological and pathophysiological conditions [7,8]. Moreover, many space instruments require that the cryocooler system possess a very high level of reliability. This need for high reliability calls for some form of redundancy to be incorporated. One common implementation is standby redundancy. The thermal connection to the redundant cooler should be low [9] until the primary unit breaks down. However, when the standby unit is needed in case of the breakdown of the primary unit, the thermal conductance should be high. Similar thermal behavior is essential for the connection between equipment and space radiators [10–12].

Unifying these examples is the use of a thermal switch, the conductance of which can be changed rapidly. In the "off" state, the heat transfer is minimized, whereas in the "on" state it is maximized in order to exchange heat rapidly with the heat sink or source. Such a switch can be constructed by having two plates with a small gap between them [13]. The conductivity across the gap increases dramatically when the content is changed from a vacuum by a gas [14] or by replacing it with a liquid. The gas pressure can be controlled actively or passively by an evaporator [15] or sorption cells [13,16].

To increase the heat flux density per base area, interleaving fins can be used. Rows of fins are attached on the two aforementioned plates in a staggered configuration. Previous research on interleaved fins has explored the effective thermal resistance across the base plates as a function of the fin dimensions, assuming uniform temperature along

*m.a.j.vanlimbeek@utwente.nl.

the length of the fin. This assumption requires high thermal conductivity of the fin compared to the gas and a further requirement is to have a low fin aspect ratio. Studies have been carried out at both cryogenic temperatures [17,18] and room temperature [19,20].

Although fins are an efficient way to increase heat exchange to the surroundings, they can lose their efficiency when the fins cool down in the longitudinal direction. This effect can be characterized by the Biot number of the fin: $\mathrm{Bi} = hL/k$, where h is the heat-transfer coefficient, L the length of the fin, and k the thermal conductivity. For $\mathrm{Bi} \ll 1$, the conduction in the fin can easily supply heat toward the cooling edges and no gradients occur, whereas for $\mathrm{Bi} \gg 1$ the opposite holds and the fin has a nonuniform temperature profile. Although, here, the heat-transfer coefficient is associated with convective transport toward the far-field temperature T_∞, we expect that in the present case of two opposing staggered fin arrays, similar behavior can be expected. Indeed, when replacing h by purely conduction over a gas-filled gap, we obtain $\mathrm{Bi}^* = k_g L/(k_s D)$, where D denotes the (uniform) gap thickness and the subscripts g and s refer to the gas and solid domains. What differs from the classical fin, however, is that here T_∞ is now the *local* temperature of the opposing fin, in this way coupling the two sides of the thermal link.

In this study, we develop an analytical one-dimensional (1D) model, which is validated by numerical solutions of the problem. We identify a more accurate Biot number and find that indeed the cooling starts to be relevant when this number is of order unity. Several ways are then explored to test the applicability of the model and in which parameter range the model loses accuracy. We also provide an expression for the heat flux across the thermal link, which is more relevant for the design. Finally, we test the gap experimentally in a range where the fins suffer from cooling, finding good agreement with our analytical prediction.

II. PROBLEM DESCRIPTION AND APPROACH

The thermal link is made up by two opposing plates with staggered fins (see Fig. 1). In between them is a gap of width $\hat{D}$, filled with a gas of conductivity $\hat{k}_g$, where the hat symbols are used to indicate dimensional quantities. The hot plate and cold plate of the stack are separated by a distance $\hat{\mathcal{L}}$. To increase the effective area, fins of width $\hat{W} - \hat{D}$ are attached on both plates in the space between them. The fins extend in the z direction much further than the gap separation, allowing the fins to be treated as quasi-two-dimensional (2D). Although, in general, the spacing and length can be chosen freely, here we restrict ourselves to the case of a constant separation $\hat{D}$. The fins start from a position $\hat{\delta}$ from the top or bottom of the stack. The region in which heat is exchanged is then $\hat{L} = \hat{\mathcal{L}} - 2\hat{\delta}$. Figure 1 shows this geometry. Many fins are positioned next to each other in the y dimension with spacing $2\hat{W}$. The hot plate is at $\hat{T} = \hat{T}_h$ and the cold plate at $\hat{T} = \hat{T}_c$ and they are made of a material that has a thermal conductivity $\hat{k}_s$. We thus identify four geometrical parameters, namely $\hat{\mathcal{L}}$, $\hat{\delta}$, $\hat{W}$, and $\hat{D}$, and three parameters related to the heat transfer: the conductivities of the gas $\hat{k}_g$ and solid $\hat{k}_s$ and the temperature difference between the hot and cold plate. We are interested in the temperature profile and the heat transfer between the plate, depending on the aforementioned parameters. Let us now outline the procedure to describe the heat transfer analytically, without the need for a full quasi-2D numerical simulation.

A. Isothermal fins

Similar to the classical problem of a single fin in an infinite fluid (see Ref. [21], Sec. 2.7), in the limit of $\hat{k}_s \to \infty$, we expect no temperature gradients to emerge into the fin. The heat exchanged, $\hat{Q}$, is then simply $-\hat{k}_g \hat{A} \Delta\hat{T}/\hat{D}$, where $\hat{A}$ is the fin area. Consider a array of interleaving fins on a plate of size $\hat{Z} \times \hat{Y}$. One finds, for the total area, that $\hat{A} = (\hat{Y}/2\hat{W})2(\hat{W} + \hat{\mathcal{L}} - 2\hat{\delta} - \hat{D})\hat{Z}$ and one obtains for the heat flux $\hat{q}'' = \hat{Q}/(\hat{Z}\hat{Y})$:

$$\hat{q}'' = -(\hat{T}_h - \hat{T}_c)\hat{k}_g \frac{\hat{W} + \hat{\mathcal{L}} - 2\hat{\delta} - \hat{D}}{\hat{D}\hat{W}}. \tag{1}$$

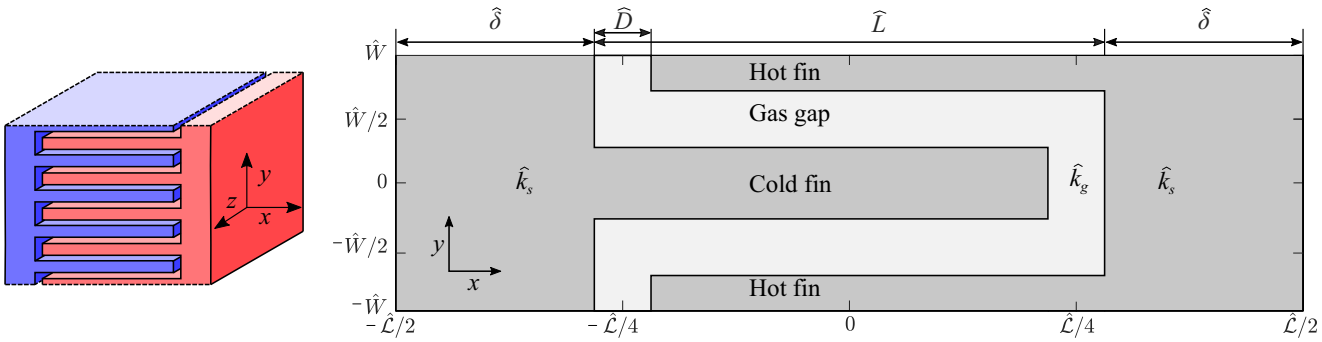

FIG. 1. A sketch of a stack of staggered fins (left) and the geometry of a single pair of fins (right). The stack extends in the y direction, whereas the fins extend in the z direction.

This solution is used as a reference to compare with the case in which the fin is subject to nonisothermal effects, which is now discussed.

B. Nonisothermal fins

Let us now sketch the solution for nonisothermal fins. The slenderness of the fins prompts one to use a 1D model, similar to the classical fin problem. We study a single pair of fins, for which we find a profile $\hat{T}(x)$ for the temperature in the fin at the cold plate. Similarly, for the fin at the hot plate we have the profile $\hat{\mathcal{T}}(\hat{x})$. We then use the temperature difference $\hat{\Theta}(\hat{x})$ between them, as the heat exchanged at any position in the fin is proportional to $\hat{\Theta}$. The problem is described by two coupled heat equations, which require four boundary conditions to be solved. The problem is solved in the following section.

III. MODELING COOLING IN THE FINS

Depending on the length scales and material properties, we explore the most simple solution to the problem, without introducing too many errors compared the full 2D (numerical) calculation. Let us first investigate the conditions in which a 1D approach is applicable. Since, here, we are studying a steady-state situation without any heat sources, the heat equation in the domain reads

$$\nabla \cdot \vec{j} = 0, \tag{2}$$

where $\vec{j} = \hat{k}\nabla\hat{T}$, the heat flux that is modeled using Fourier's law. In the current study, we assume $\hat{k}$ to be independent of the temperature. Considering a single fin now, we can rescale the $\hat{x}$ and $\hat{y}$ coordinate with the length $\hat{\mathcal{L}}$ and width $\hat{W} - \hat{D}$ of the fin as $\hat{x} = \hat{\mathcal{L}}\bar{x}$ and $\hat{y} = (\hat{W} - \hat{D})\bar{y}$,= obtaining

$$\hat{k}_s\left(\partial_{\hat{x}\hat{x}}\hat{T} + \partial_{\hat{y}\hat{y}}\hat{T}\right) = \hat{k}_s\left(\partial_{\bar{x}\bar{x}}\hat{T} + \frac{\hat{\mathcal{L}}^2}{(\hat{W} - \hat{D})^2}\partial_{\bar{y}\bar{y}}\hat{T}\right) = 0, \tag{3}$$

which acts on the domain $x, y = [0, 1]$. Inspection shows that for large $\hat{\mathcal{L}}^2/(\hat{W} - \hat{D})^2$, the gradients in the $\bar{y}$ direction become small compared those in the $\bar{x}$ direction. This prompt us to assume $\hat{T}(\hat{x}, \hat{y}) \approx \hat{T}(\hat{x})$, which we will validate *a posteriori*. Equation (2) is now integrated over a small slice of the fin. The slice extends over the full width of the fin $\hat{W} - \hat{D}$ and has a thickness $\Delta\hat{x}$, so we obtain, using the Gauss theorem in two dimensions,

$$\int_v \nabla \cdot \vec{j}\, dV = \oint \vec{j} \cdot \vec{n}\, d\ell = 0,$$

$$\hat{k}_s(\hat{W} - \hat{D})\left(\frac{d\hat{T}(\hat{x} + \Delta\hat{x})}{d\hat{x}} - \frac{d\hat{T}(\hat{x})}{d\hat{x}}\right) + 2\Delta\hat{x}\hat{q}_{\text{gap}} = 0. \tag{4}$$

Evaluating the limit of $\Delta\hat{x} \to 0$ yields

$$\hat{k}_s(\hat{W} - \hat{D})\frac{d^2\hat{T}(\hat{x})}{d\hat{x}^2} + 2\hat{q}_{\text{gap}} = 0, \tag{5}$$

where a Taylor expansion is used. Here, $\hat{q}_{\text{gap}}$ is the heat exchanged with the opposing fin, which we model as $-(\hat{k}_g/\hat{D})[\hat{T}(\hat{x}) - \hat{\mathcal{T}}(\hat{x})]$. Using a similar procedure for the opposing fin gives us the following coupled equations for the temperature profiles $T(\hat{x})$ and $\mathcal{T}(\hat{x})$:

$$\begin{aligned}\hat{k}_s(\hat{W} - \hat{D})\frac{d^2\hat{T}}{d\hat{x}^2} - \frac{2\hat{k}_g}{\hat{D}}(\hat{T} - \hat{\mathcal{T}}) = 0,\\ \hat{k}_s(\hat{W} - \hat{D})\frac{d^2\hat{\mathcal{T}}}{d\hat{x}^2} - \frac{2\hat{k}_g}{\hat{D}}(\hat{\mathcal{T}} - \hat{T}) = 0.\end{aligned} \tag{6}$$

The coupled system of equations is subject to the following boundary conditions: the temperature profiles should satisfy the Dirichlet boundary condition $\hat{T}(-\mathcal{L}/2) = \hat{T}_c$ or $\hat{\mathcal{T}}(\mathcal{L}/2) = \hat{T}_h$, respectively. The problem is closed by noting that heat is conserved in the system, from which we find that $k_s(d\hat{T}/dx)|_{-\mathcal{L}/2} = k_s(d\hat{\mathcal{T}}/dx)|_{\mathcal{L}/2}$.

It is interesting to investigate similarities with Sec. 2.7.4 in Ref. [21] to validate the 1D model. The present model can lose accuracy when the Biot number for the width of the fin $\text{Bi}^\dagger = h(\hat{W} - \hat{D})/\hat{k}_s = \hat{k}_g(\hat{W} - \hat{D})/(\hat{k}_s\hat{D})$ exceeds 1. Here, we use $h = \hat{k}_g/\hat{D}$ for the heat-transfer coefficient over the conducting gas gap. When $\text{Bi}^\dagger > 1$, gradients occur in the cross-section plane. However, for the slender fins considered here, gradients in the x direction will dominate corrections arising from cooling in the y direction. We now nondimensionalize the spatial dimension and lengths by the thickness $\hat{\mathcal{L}}$ of the stack, $\hat{x} = x\hat{\mathcal{L}}$, and the temperatures using the boundary temperatures [e.g., $\hat{T} = (\hat{T}_h - \hat{T}_c)T + \hat{T}_c$]. For thermal conductivities, we rescale by the conductivity of the solid: $k = \hat{k}_g/\hat{k}_s$. Let $\Theta = T - \mathcal{T}$ and $C^2 = (4\hat{k}_g\hat{\mathcal{L}}^2)/[\hat{k}_s\hat{D}(\hat{W} - \hat{D})]$; we then obtain

$$\Theta'' - C^2\Theta = 0 \tag{7}$$

and

$$T'' - \frac{1}{2}C^2\Theta = 0, \quad \mathcal{T}'' + \frac{1}{2}C^2\Theta = 0, \tag{8}$$

where we use primes to represent the derivatives. Let the center of the stack be at $\hat{x} = 0$. We then find, for the boundary conditions, $T(-1/2) = 0$, $\mathcal{T}(1/2) = 1$, and $T'(-1/2) = \mathcal{T}'(1/2)$. The solution for Θ is then $\alpha\exp(Cx) + \beta\exp(-Cx)$.

Theorem 1: The symmetry of the geometry results in Θ being an even function.

Proof: Let Θ and $\tilde{\Theta}$ be solutions to Eq. (3) and let $\tilde{\Theta}(x) = \Theta(-x)$. We then find $\Theta(-x)'' - C^2\Theta(-x) = 0 \rightarrow \tilde{\Theta}(x)'' - C^2\tilde{\Theta}(-x) = 0$. At $x = 0$, the two solutions coincide: $\Theta(0) = \tilde{\Theta}(0)$. Hence, from uniqueness, we deduce that $\Theta(x) = \tilde{\Theta}(x) = \Theta(-x)$ is an even function. ■

In order for Θ to be even, we find that $\alpha = \beta \equiv 2\Theta_0$, which yields

$$\Theta = \Theta_0 \cosh(Cx). \tag{9}$$

Substitution of Eq. (7) into Eq. (8) yields for T, after integrating twice,

$$T = \frac{1}{2}\Theta_0 \cosh(Cx) + a + bx, \tag{10}$$

where we find three integration constants: a, b, and Θ_0. First, we use continuity of flux in a single fin to find that, per pair of opposing fins, i.e., per $2W$,

$$-(W-D)T'|_{-1/2+\delta} = 2\int_{-1/2+\delta}^{1/2-\delta} \frac{k}{D}\Theta\, dx - (W-D)T'|_{1/2-\delta}. \tag{11}$$

The left-hand side denotes the flux at the base of the fin, the integral the flux crossing the gap sideways, and the last term the heat exchange at the tip of the fin. Using Eq. (10), one obtains

$$\begin{aligned} b = {} & \Theta_0 \frac{C}{2}\sinh(\mathcal{C}) - \frac{2}{W-D}\frac{k}{D}\Theta_0 \frac{2}{C}\sinh(\mathcal{C}) \\ & - \frac{k}{D}\Theta_0 \cosh(\mathcal{C}), \end{aligned}$$

where $\mathcal{C} = C(\frac{1}{2} - \delta)$. Next, we approximate the flux through the support of the fins as $2W\left[T(-\frac{1}{2}) - T(-\frac{1}{2} + \delta)\right]/\delta$. This flux is equal to the sum of the heat entering the fin and directly flowing from the base into the tip of the opposing fin: $-(W-D)T'|_{-1/2+\delta} + (W-D)(k/D)\Theta(-\frac{1}{2} + \delta)$. In this way, we can express a as follows:

$$\begin{aligned} a = {} & -\frac{1}{2}\Theta_0 \cosh(\mathcal{C}) - b\left(-\frac{1}{2} + \delta\right) \ldots \\ & - \delta\frac{W-D}{2W}\left(\Theta_0 \frac{C}{2}\sinh(\mathcal{C}) - b\right) \\ & + \delta\frac{W-D}{2W}\frac{k}{D}\Theta_0 \cosh(\mathcal{C}). \end{aligned} \tag{12}$$

Finally, we can close the problem by evaluating the solution at $x = -1/2$, where we find $T = 0$, to obtain the value of Θ_0. Note that Θ_0 is the temperature difference between the fins at $x = 0$. The symmetry of the two opposing fins allows us to write $\Theta_0 = 2(T(x = 0) - 1/2)$, where $1/2$ represents $(T_h + T_c)/2$. We then find $a = 1/2$, from which one can obtain Θ_0 more easily using Eq. (12). Θ_0 is therefore a measure for the amount of cooling in the system: in the isothermal limit, we find that $\Theta_0 = -1$.

We now arrive at the following equation for the temperature field:

$$T = \begin{cases} -\left(x + \frac{1}{2}\right)\frac{W-D}{2W}\left(\Theta_0 \frac{C}{2}\sinh(\mathcal{C}) - b\right), & -\frac{1}{2} \leqslant x < -\frac{1}{2} + \delta, \\ \text{Eq. (10)}, & -\frac{1}{2} + \delta \leqslant x < \frac{1}{2} - \delta, \\ 1 - \left(x + \frac{1}{2}\right)\frac{W-D}{2W}\left(\Theta_0 \frac{C}{2}\sinh(\mathcal{C}) - b\right), & -\frac{1}{2} - \delta \leqslant x < \frac{1}{2}. \end{cases} \tag{13}$$

A similar procedure can be followed to obtain $\mathcal{T}$. The dimensional form of Eq. (13) can be obtained easily by rescaling the x-coordinate and the temperature. Note that in our analysis we extend the fin toward $x = 1/2 - \delta$. In principle, the upper boundary of the integral would be $x = 1/2 - \delta - D$ to treat the finite-size gap accurately. However, the solutions simplify greatly when we ignore this, as the integral becomes symmetric around $x = 0$. The numerical validation in Sec. IV will show that this simplification does not have too much impact on the accuracy of the model.

Let us now consider the (dimensional) heat flux exchanged per frontal unit area, this is from an application perspective the quantity of interest. We find, for the width of a single pair of fins,

$$2Wq'' = \frac{k}{D}\Theta_0\left(\frac{4}{C}\sinh(\mathcal{C}) + 2(W-D)\cosh(\mathcal{C})\right), \tag{14}$$

or in dimensional units,

$$2\hat{W}\hat{q}'' = \Delta\hat{T}\frac{\hat{k}_g\hat{\mathcal{L}}}{\hat{D}}\Theta_0\left(\frac{4}{C}\sinh(\mathcal{C}) + 2\frac{\hat{W}-\hat{D}}{\hat{L}}\cosh(\mathcal{C})\right), \tag{15}$$

from which $\hat{q}''$ can be obtained. It is interesting to expand Eq. (15) in the limit of $C \to 0$, as it reduces correctly to Eq. (1): $\hat{q}'' = \Delta\hat{T}(\hat{k}_g\hat{\mathcal{L}}/2\hat{W}\hat{D})\Theta_0\left(4\left(\frac{1}{2} - (\hat{\delta}/\hat{\mathcal{L}})\right) + 2(\hat{W} - \hat{D})/\hat{\mathcal{L}}\right) + \mathcal{O}(C^2) + \ldots$.

IV. RESULTS

The analytical model is first validated using numerical solutions of the problem and employing the commercial software package COMSOL [22]. The steady-state heat equation is solved by a finite-element method on a triangular grid. We consider one half of a pair of opposing fins inside a large stack, avoiding any edge effects. The hot and cold faces have Dirichlet boundary conditions where the longitudinal boundaries satisfy the no-flux condition. The solid-gas boundaries satisfy continuation of heat flux and a no-jump condition in temperature.

Two cases are presented in Fig. 2 for $C = 0.9$ and 9.1, where the gas conductivity is varied. It can clearly be seen that the isotherms in Fig. 2(a), shown by the colored lines, lie mostly within the gas gap. Strong gradients appear in panel (b), however, as expected since $C > 1$. In the center, the temperature difference between the two profiles, Θ_0, is added. We find that for isothermal fins it is close to unity, while it decreases when significant gradients occur in the film, since the conductivity of the gas increases.

We now test how trustworthy C is in predicting the occurrence of nonisothermal fins. We vary the parameters W, $\hat{\mathcal{L}}$, D, $\hat{k}_s$, and $\hat{k}_g$ independently and study the behavior of Θ_0, which is presented in Fig. 3. Independent through which parameter C is changed, the behavior of Θ_0 is the same. We clearly find that for $C < 0.1$ the fins are isothermal, whereas for $C = [0.1, 1]$, Θ_0 goes from -1 to -0.8 in that regime. Increasing C further results quickly in a decrease in effectiveness, where from $C \approx 10$ no significant temperature difference between the fins is found. The behavior of Θ_0 is fitted accurately using a single fitting parameter ζ:

$$\Theta_0 = \frac{1}{2}\left\{\mathrm{erf}\left[\log_{10}(C^2) + \zeta\right] - 1\right\}, \tag{16}$$

as presented in Fig. 3, where we find that $\zeta = -0.7$. Equation (16) is not required for the model developed in Sec. III, from which Θ_0 can also be obtained.

So far, we have focused purely on numerical results, so let us now focus on comparing the solutions to the model developed earlier in Sec. III. From the numerical solution for $C = 2.9$ and $\delta = 0.22$, we obtain the profiles in the hot and cold fin, as shown in Fig. 4. Focusing on the blue temperature profile T of the cold fin, we use Eq. (13), plotted in purple, yellow, and green. Although the agreement looks good for all pieces, we quantify this by comparing the following properties. First, we compare the difference in C and Θ_0 by fitting the temperature difference of the numerical solution using Eq. (9); we then compare the fit with the expression for C and Θ_0. Second, we compare the difference of the fin profiles between the numerical and analytical models using the relative error

$$e_{\mathrm{fin}} = \frac{1}{\Delta x}\frac{2}{\bar{T}_{\mathrm{num}} + \bar{T}_{\mathrm{Eq.\ (6)}}}\sum_i \left|T_{\mathrm{num}} - T_{\mathrm{Eq.\ (6)}}\right|, \tag{17}$$

where the sum is taken over all positions i in the fin, being spaced by Δx, and the bar represents the mean temperature of the fin.

For an application perspective, the error in the heat flux between the plates is more relevant and can be expressed as $q_{\mathrm{num}}/q_{\mathrm{Eq.\ 10}}$. We now vary the conductivity ratio $k \equiv \hat{k}_g/\hat{k}_s$

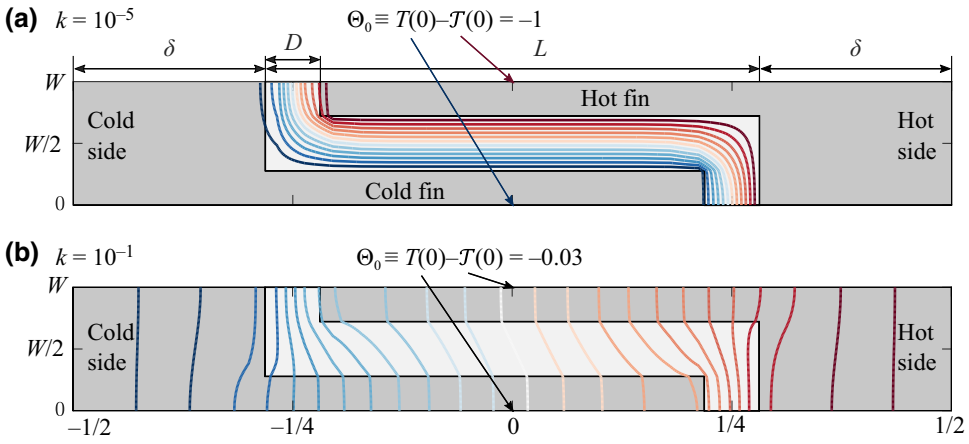

FIG. 2. The numerical solution for $D = 0.0625$, $\delta = 0.22$, and $W = 0.14$. The results for a low-conductivity gas of $k = \hat{k}_g/\hat{k}_s = 10^{-5}$ are displayed in panel (a), whereas panel (b) is solved with $k = 10^{-1}$, resulting in $C = 0.9$ and 9.1, respectively. The colored lines indicate isotherms between $T = 0$ (blue) and 1 (red).

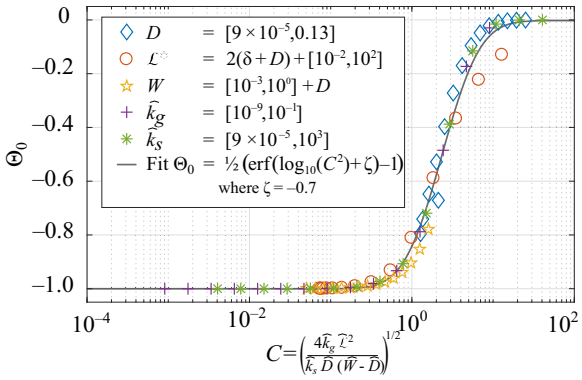

FIG. 3. The temperature difference Θ_0 between the two fins. Rescaling the parameters using C reveals a single curve for which Eq. (16) is fitted (black line).

as well as the slenderness of the fins W/L, while keeping the ratio between W and D constant. Figure 5 shows the performance of the model varying $k = [10^{-5}, 10^{-1}]$ and $\hat{\mathcal{L}} = [3.2, 32]$ mm. The numerical data are evaluated in the center of the hot and the cold fin, after which the difference is fitted by Eq. (9), with C and Θ_0 as fitting parameters. For large C, the data are fitted in log space for numerical stability. The results are presented in Fig. 5, where the error in C is the ratio between C (as defined in Sec. III) and the fit. We obtain good agreement over the complete phase space. The error in Θ_0 is obtained by dividing the numerical fitting parameter by the value from the analytical model developed in Sec. III. We find good agreement for the parameter space where $\Theta_0 > -0.05$. The analytical model, however, starts to underestimate Θ_0 for $C > 20$. For fixed C, we can follow the phase space from high $L/(W-D)$ down to large k. In doing so, the model and simulations lose agreement as the error in Θ_0 increases. The two panels on the right show the error in the heat flux, only deviating more than 5% for $\Theta_0 > -0.05$ as well. Evaluation of Eq. (17) shows that the mean difference between the numerical temperature profiles and the analytical model is smaller than 3% for the complete phase space studied. The good agreement found between the analytical model and the numerical results demonstrates the robustness as well as the accuracy of our 1D model.

V. DISCUSSION

In the previous section, we develop and validate an analytical model to calculate the temperature profile in the fins of a heat switch and give predictions for the heat flux. The parametric study for $D, \hat{\mathcal{L}}, W, \hat{k}_g$, and $\hat{k}_s$ shows that non-isothermal effects can be understood by the use of C. The fit Eq. (16) is able to capture the behavior of Θ_0 up to a single fitting constant: ζ. We find that the mesh generated for the numerical study becomes too coarse for $\hat{\mathcal{L}} > 8$, the results for which are therefore neglected in the fitting procedure. The fit is of great value in a quick evaluation of the heat exchange across the heat switch: Eq. (15) can now be easily be evaluated by the system parameters, ΔT and Eq. (16). Let us stress that it is not a fitting parameter to the model developed in Sec. III.

Let us briefly comment here on the fit parameter b. Additional simulations of the problem make clear that b is a function of the thickness of the material δ. By fixing the fin geometry and varying C through k, we find that $\zeta(0) = -0.4$ for $\delta \to 0$ and, more generally,

$$\zeta \approx \frac{-0.42}{1 - 1.7\delta}, \tag{18}$$

which is valid for $\delta = [0, 15]$. This results in a shift of the function along the C axis, since C is based on the complete domain. Basing C on the fin length does not, however, eliminate the δ dependency of ζ completely, as the thickness δ of the solid material itself acts as an insulating layer. For practical applications, therefore, one wants to minimize the thickness δ for this reason and use $\zeta \approx -0.4(1 + 1.7\delta)$ as an approximation of Eq. (18) for moderate δ.

From the validation study presented in Fig. 5 of the analytical model, we obtain good agreement in the regions of significant exchange between the fins. First, the fitted values for C and Θ_0 agree to within a few percent with the analytical expression [see Eq. (7)], as well as the deviations in the temperature profiles. We only encounter strong deviations for $C > 50$ or $k > 0.05$. In those situations, however, the effectiveness of the fins is greatly reduced anyway: the length of the fins acts, in fact, as an insulating layer, negating the effect of the additional surface area

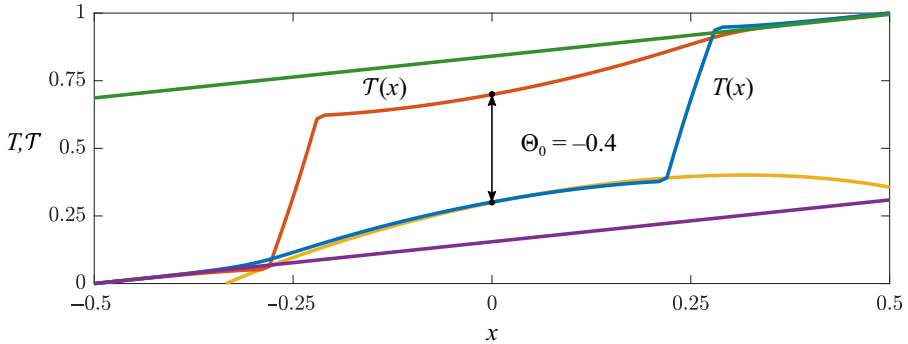

FIG. 4. A comparison between the numerical solutions of T (blue) and $\mathcal{T}$ (red) and the analytical model for $C = 2.9$. Θ_0 is evaluated to be -0.4. The analytical model is a piecewise function of Eq. (10) (yellow), which describes the profile in the fin, and Eq. (13).1 (purple) and (13).3 (green) for the profiles in the base fins.

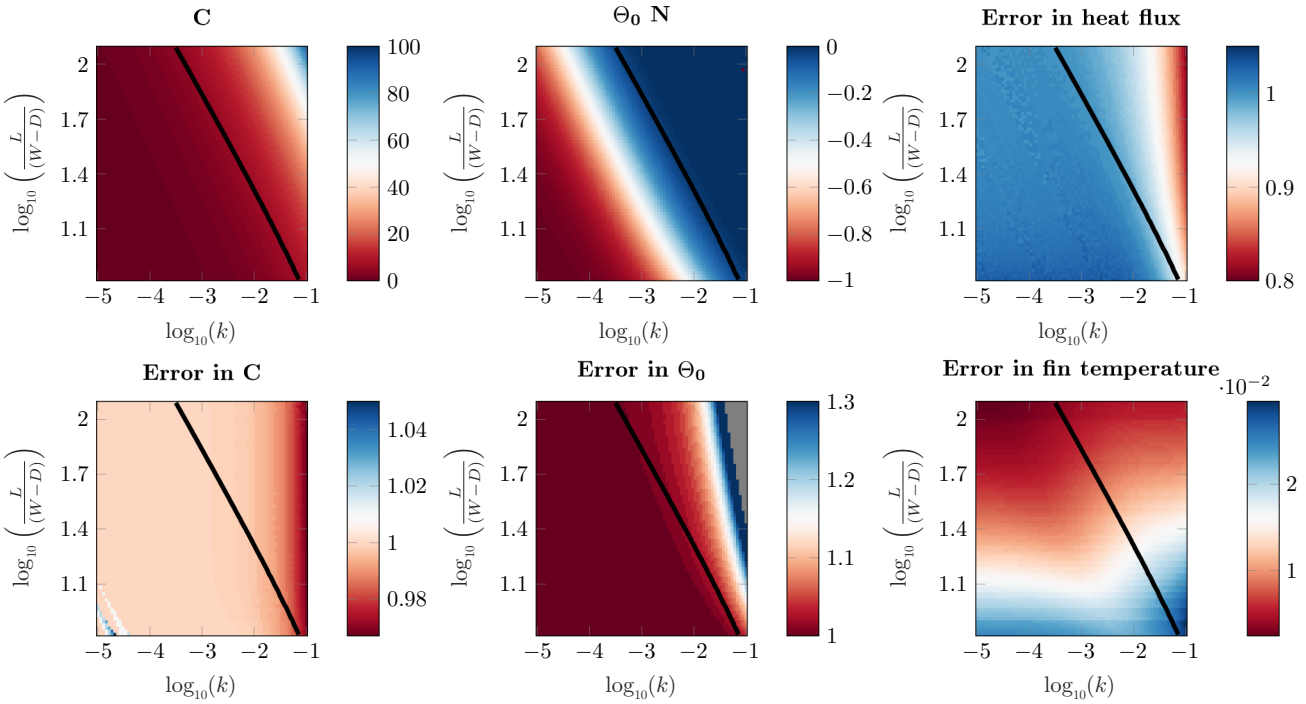

FIG. 5. The accuracy of the analytical model is tested for $\hat{\mathcal{L}} = [3.2, 32]$ mm, $\hat{\delta} = 0.7$ mm, $\hat{W} = 0.45$ mm, and $\hat{D} = 0.2$ mm, from which C (top left panel) and Θ_0 (top middle panel) are presented. The errors are calculated using the methods in the text. The values of $-\Theta_0 < 0.05$ are left of the black lines, whereas the gray area denotes errors exceeding 1.3.

in this way. Our model thus performs best in the parameter space that is relevant to the problem. We speculate that deviations occur for two reasons. First, for constant C, less slender fins suffer from cooling in the perpendicular directions and the 1D model becomes less accurate. Second, for increasing k, the isotherms in the gap become less parallel to the side walls of the fin [see Fig. 2(b)]. As a result, the flux lines $-k\nabla T$ are no longer normal to the wall, which is not included in the analytical model. Despite these two effects, the performance of the analytical model is still good.

A. Comparison with experiments

Finally, we compare our model with the experimental measurements performed in our laboratory at ambient [20] and cryogenic [23] temperatures. Let us briefly elaborate on the relevant details of the setup. The heat switch is constructed out of a sintered titanium alloy (Ti_6Al_4V grade 5), having 49 rows of interleaving fins. The switch operates between the "on" state, where a high heat transfer is required, and the "off" state by removing the gas in the gas gap. Although the gas conductivity is at most weakly dependent on the ambient pressure for bulk values, it can be reduced drastically as a result of the confinement by the fins. For pressures below 100 Pa, the gas must be treated as a Knudsen gas. Krielaart *et al.* [20] studied helium, nitrogen, and hydrogen gas at room temperature ($T_m = 294$ K), whereas Vanapalli *et al.* [23] studied helium and nitrogen at cryogenic conditions. For the cryogenic measurements, the setup was operating at an mean temperature of 117.5 K, resulting in a bulk lower conductivity of the gas, as well as that of the solid compared to the ambient case. Evaluation of C for the "on" states yields $C = 1.8$ for nitrogen, and $C = 4.5$ and 4.1 for hydrogen and helium, respectively, at room-temperature conditions, whereas $C = 3.8$ is found for both gases at cryogenic conditions. For all "on" states, one can thus expect a non-negligible cooling effect, which reduces the heat-transfer rate.

As shown in both references [20,23], proper modeling of the full experimental setup requires the inclusion of a contact resistance at both sides of the heat switch (see, e.g., [24]). Graphite foil of thickness 350 μm and thermal paste were added to provide good thermal contact with the segments controlling the hot and cold boundary conditions [23]. To obtain good agreement with the model, the total contact resistance is found to be around $1/(2 \times 10^3)$ K/W, which can be estimated using ℓ/k_c. Here, $k_c = 0.2$ is the conductivity of the thermal paste (Apizon N) and $\ell \approx 100$ μm the typical layer thickness. This estimate is reasonable as it represents the roughness of the heat switch, which was made out of sintered titanium alloy grains having a diameter of 100 μm. Since graphite is a good thermal conductor, it does not contribute to the contact resistance.

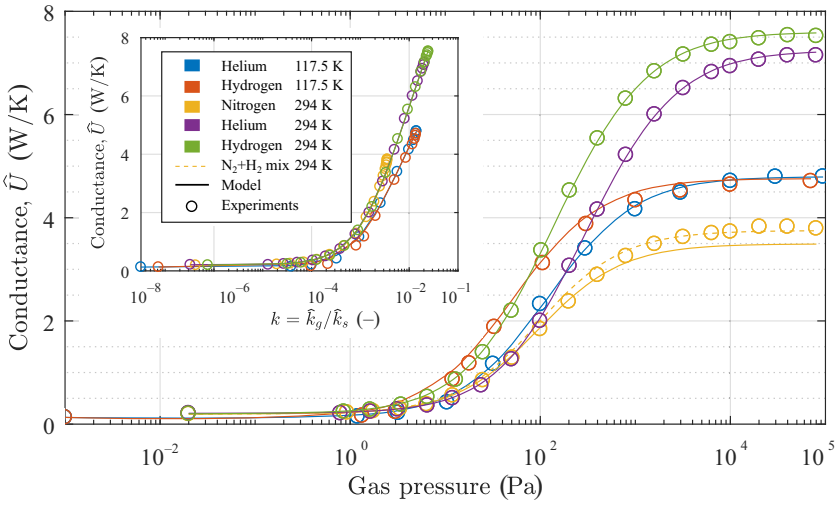

FIG. 6. A comparison of the model (solid lines) with experiments. The conductivity ratio k is varied by reducing the pressure in the heat switch, for which the system is subject to Knudsen effects.

The thermal contact resistance results in a reduction of the total heat transfer of 40% for the highest gas conductivities measured: indeed, for those cases, the thermal resistance of the heat switch becomes of the same order as the contact resistance, resulting in a significant temperature drop across the thermal paste layer.

The comparison of the experimental measurements with the analytical model is presented in Fig. 6. Both the helium and hydrogen measurements show good agreement with the model, whereas the largest discrepancy is found for nitrogen measurements, being approximately 10%. This experiment was done after the hydrogen measurements (laboratory records and private communication with the authors of Ref. [20], October 2019), which is known to diffuse into titanium alloys [25]. It is expected that hydrogen gas will still diffuse out of the metal when measuring nitrogen, increasing the thermal conductivity. A gas thermal conductivity of 1.175 times that of pure nitrogen gas (dashed line) shows good agreement. This is equal to a mass fraction of 5% and a weight fraction of 1%, using the model of Wassiljewa [26] and its extension by Mason and Saxena [27]. We thus show that a design optimal for ambient testing conditions does not necessarily guarantee the same performance at cryogenic conditions, since not only the physical properties change, but also the impact of the nonisothermal effect changes. However, our model captures these effects accurately and yields good predictions of the thermal conductance.

B. Edge effects

We treat fins extending far in the z direction as well as those being in the center of the stack. In this way, we ignore effects originating from the supporting walls, joining the two sides of the heat exchanger. Here, we sketch when edge effects can become significant: the top and bottom fin of the stack can be in direct contact with an external temperature field. Here, the relatively good conducting fin will take the profile as imposed by the boundary conditions. The next (opposing) fin will be shielded to some extent by the lower conductivity in the gap. To reduce the heat flow from this configuration, the top and bottom fins are separated by a gas gap from an outside supporting wall (see Ref. [20]; see also Refs. [13,19,28]). This changes the boundary condition from Dirichlet to Neumann: any influence on the profile of the fins can now be characterized by another Biot number $\mathrm{Bi}_{\mathrm{wall}} = \hat{h}_{\mathrm{wall}}(\hat{W} - \hat{D})/\hat{k}_s$, where $\hat{h}_{\mathrm{wall}}$ is the heat-transfer coefficient from the supporting wall into the fin. A similar analysis can be used for the side edges of the fins (i.e., where the fins end in the z direction). Here, the temperature profiles are influenced by either direct contact (Dirchlet) or a heat flux (Neumann) over a length scale $\hat{\mathcal{L}}$ (see Ref. [21], Sec. 3.1). Again, a Biot number using $\hat{\mathcal{L}}$ determines the strength in the case of a heat flux.

C. Transient effects

While we study the steady-state behavior, let us finally briefly discuss the expected behavior of the transient operation. When the system of interleaving fins is used in a heat switch for switching between the "on" and "off" states, the corresponding cooling and heating of the fins themselves becomes relevant. Intuitively, one can expect the "off" state to be in the isothermal regime. Recovery from a previous "on" state is thus determined by heat diffusing from the hot or cold side to the tip of a fin. The (dimensional) diffusive time scale is then $\hat{\tau}_{\mathrm{rec}} = \hat{L}^2\hat{\rho}\hat{c}_p/\hat{k}_s$, where $\hat{\rho}$ and $\hat{c}_p$ are the density and specific heat of the solid. When the switch is turned "on" again, heat is first exchanged locally, for which we use the thermal time scale for transient heat transfer: $\hat{\tau}_{\mathrm{trans}} = \hat{k}_s\hat{\rho}\hat{c}_p/(\hat{k}_g/\hat{D})^2$ [21]. It is interesting to look at the ratio between the two, for which we find $(\hat{k}_g/\hat{k}_s \cdot \hat{D}/\hat{L})^2$. We then find that this gives a ratio of time spans for cycling between "on" and "off" states, provided that the fluid-flow time scale is fast. This cannot always be ensured, as the

viscous effect can start to play a role for small length scales. This trade-off is important if one is interested in transient operation of the fins.

VI. CONCLUSION

We find solutions to interleaving fins where the fins may develop thermal gradients. The performance of the fin depends strongly on whether or not this effect takes place. We find that the nondimensional parameter $C = \left[(4\hat{k}_g\hat{\mathcal{L}}^2)/[\hat{k}_s\hat{D}(\hat{W}-\hat{D})]\right]^{1/2}$ characterizes this well, collapsing numerical solutions of the problem when varying C through the different parameters over 6 orders of magnitude. For $C < 1$, the thermal gradients may be neglected and one should use Eq. (1). In the other cases, we develop and test an analytical model that shows excellent agreement with both numerical solutions to the problem for a large parameter space as well as with experiments. Next, we provide several easy-to-use approximations aimed at system optimization for engineering purposes. Our work offers an analytical solution to find the heat flux for this type of heat exchanger and may provide valuable insights for the design and optimization of such systems once the thermal properties are known.

[1] W. Stautner, R. Chen, A. Comment, and E. Budesheim, An efficient liquid helium/gas-gap switch allowing rapidly servicing low-temperature dynamic nuclear polarization systems, IOP Conf. Ser.: Mater. Sci. Eng. **502**, 012162 (2019).

[2] Marc Medrano, M. O. Yilmaz, M. Nogués, I. Martorell, Joan Roca, and Luisa F. Cabeza, Experimental evaluation of commercial heat exchangers for use as PCM thermal storage systems, Appl. Energy **86**, 2047 (2009).

[3] Albert Castell, Martin Belusko, Frank Bruno, and Luisa F. Cabeza, Maximisation of heat transfer in a coil in tank PCM cold storage system, Appl. Energy **88**, 4120 (2011).

[4] Esam M. Alawadhi and Cristina H. Amon, in *ITHERM 2000. The Seventh Intersociety Conference on Thermal and Thermomechanical Phenomena in Electronic Systems (Cat. No. 00CH37069)* (IEEE, Las Vegas, Nevada, USA, 2000), Vol. 1, pp. 283–289.

[5] Mohammed M. Farid, Amar M. Khudhair, Siddique Ali K. Razack, and Said Al-Hallaj, A review on phase change energy storage: Materials and applications, Energy Convers. Manage. **45**, 1597 (2004).

[6] G. Bonfait, I. Catarino, J. Afonso, D. Martins, M. Linder, and L. Duband, 20k energy storage unit, Cryogenics **49**, 326 (2009).

[7] G. Schneider, B. Niemann, P. Guttmann, D. Rudolph, and G. Schmahl, Cryo x-ray microscopy (1995).

[8] Gerd Schneider, Cryo x-ray microscopy with high spatial resolution in amplitude and phase contrast, *Ultramicroscopy* 75, 85 (1998).

[9] R. G. Ross, in Cryocoolers 11 (Springer, New York City, New York, USA, 2002), pp. 637–648.

[10] David C. Bugby, Jeffery T. Farmer, Brian F. O'Connor, Melissa J. Wirzburger, Elisabeth D. Abel, and Chuck J. Stouffer, in *AIP Conference Proceedings* (AIP, Huntsville, Alabama, USA, 2010), Vol. 1208-1, pp. 76–83.

[11] D. S. Glaister, D. G. T. Curran, V. N. Mahajan, and M. Stoyanof, in *1996 IEEE Aerospace Applications Conference Proceedings* (IEEE, Aspen, Colorado, USA, 1996), Vol. 2, pp. 115–127.

[12] S. Gross, Thermal coupling of equipment by interleaving fins, J. Spacecr. Rockets **7**, 489 (1970).

[13] I. Catarino, G. Bonfait, and L. Duband, Neon gas-gap heat switch, Cryogenics **48**, 17 (2008).

[14] William R. Hamburgen, John S. Fitch, and Robert A. Eustace, Interleaved-fin thermal connector, U.S. Patent No. 5,787,976 (1998).

[15] F. Romera, D. Mishkinis, A. Kulakov, and A. Torres, in *15th Int. Heat Pipe Conf., Clemson, USA* (Clemson, South Carolina, USA, 2010), pp. 25–30.

[16] J. F. Burger, H. J. M. Ter Brake, H. J. Holland, R. J. Meijer, T. T. Veenstra, G. C. F. Venhorst, D. Lozano-Castello, M. Coesel, and A. Sirbi, Long-life vibration-free 4.5 k sorption cooler for space applications, Rev. Sci. Instrum. **78**, 065102 (2007).

[17] Peter J. Shirron and Michael J. Di Pirro, Passive gas-gap heat switch for adiabatic demagnetization refrigerator, U.S. Patent No. 6,959,554 (2005).

[18] M. J. Di Pirro and P. J. Shirron, Heat switches for ADRs, Cryogenics **62**, 172 (2014).

[19] Srinivas Vanapalli, Bram Colijn, Cris Vermeer, Harry Holland, Thierry Tirolien, and Hermanus J. M. ter Brake, A passive, adaptive and autonomous gas gap heat switch, Phys. Procedia **67**, 1206 (2015).

[20] M. A. R. Krielaart, Cristian Hendrik Vermeer, and Srinivas Vanapalli, Compact flat-panel gas-gap heat switch operating at 295 K, Rev. Sci. Instrum. **86**, 115116 (2015).

[21] Adrian Bejan, *Heat Transfer*, 1st ed. (John Wiley @ Sons, Inc., New York, 1993).

[22] COMSOL AB, COMSOL *Multiphysics v. 5.2.*, Stockholm, Sweden.

[23] Srinivas Vanapalli, R. Keijzer, P. Buitelaar, and Hermanus J. M. ter Brake, Cryogenic flat-panel gas-gap heat switch, Cryogenics **78**, 83 (2016).

[24] M. Michael Yovanovich, Effect of foils upon joint resistance: Evidence of optimum thickness, AIAA Prog. Astronaut. Aeronaut. Thermal Control Radiat. **3**, 1 (1973).

[25] Jeff L. Blackburn, Philip A. Parilla, Thomas Gennett, Katherine E. Hurst, Anne C. Dillon, and Michael J. Heben, Measurement of the reversible hydrogen storage capacity of milligram Ti-6Al-4V alloy samples with temperature programmed desorption and volumetric techniques, J. Alloys Compd. **454**, 483 (2008).

[26] Alexandra Wassiljewa, Warmeleitung in Gasgemischen, Physik. Z. **5**, 737 (1904).

[27] E. A. Mason and S. C. Saxena, Approximate formula for the thermal conductivity of gas mixtures, Phys. Fluids **1**, 361 (1958).

[28] Q. S. Shu, J. A. Demko, and J. E. Fesmire, in *IOP Conference Series: Materials Science and Engineering* (IOP Publishing, Madison, Wisconsin, USA, 2017), Vol. 278, p. 012133.